

Search for the QCD critical point by NA61/SHINE at the CERN SPS

Haradhan Adhikary for the NA61/SHINE Collaboration

Jan Kochanowski University, Kielce, Poland

E-mail: haradhan.adhikary@cern.ch

Contribution to: ICNFP2021

Abstract. The existence and location of the QCD critical point is an object of both experimental and theoretical studies. The comprehensive data collected by the NA61/SHINE during a two-dimensional scan in beam momentum (13A-150A GeV/c) and system size ($p+p$, $p+Pb$, Be+Be, Ar+Sc, Xe+La, Pb+Pb) allows for a systematic search for the critical point – a search for a non-monotonic dependence of various correlation and fluctuation observables on collision energy and size of colliding nuclei. In particular, fluctuations of particle number in transverse momentum space are studied. They are quantified by measuring the scaling behavior of factorial moments of multiplicity distributions.

This contribution reviews ongoing NA61/SHINE studies to search for the critical point of the strongly interacting matter.

Keywords: critical point, second scaled-factorial moments, intermittency

1. Introduction

1.1. NA61/SHINE at CERN SPS

NA61/SHINE (SPS Heavy Ion and Neutrino Experiment) [1] is a multi-purpose facility measuring hadron production in hadron-proton, hadron-nucleus and nucleus-nucleus collisions. It is a fixed target experiment located at the H2 beam-line in the North Area of the CERN Super Proton Synchrotron (SPS). The main physics goals of the experiment are to study the onset of deconfinement and search for the critical point.

1.2. NA61/SHINE detector

The NA61/SHINE detection system [1], presented in Fig. 1, is a large acceptance hadron spectrometer with excellent capabilities in measuring charged particles. The main tracking devices are eight Time Projection Chambers, two of which are placed inside superconducting magnets, complemented by three Time-of-Flight detectors. This setup allows for precise momentum reconstruction and identification of charged particles. The high-resolution forward hadron calorimeter, the Projectile Spectator Detector (PSD),

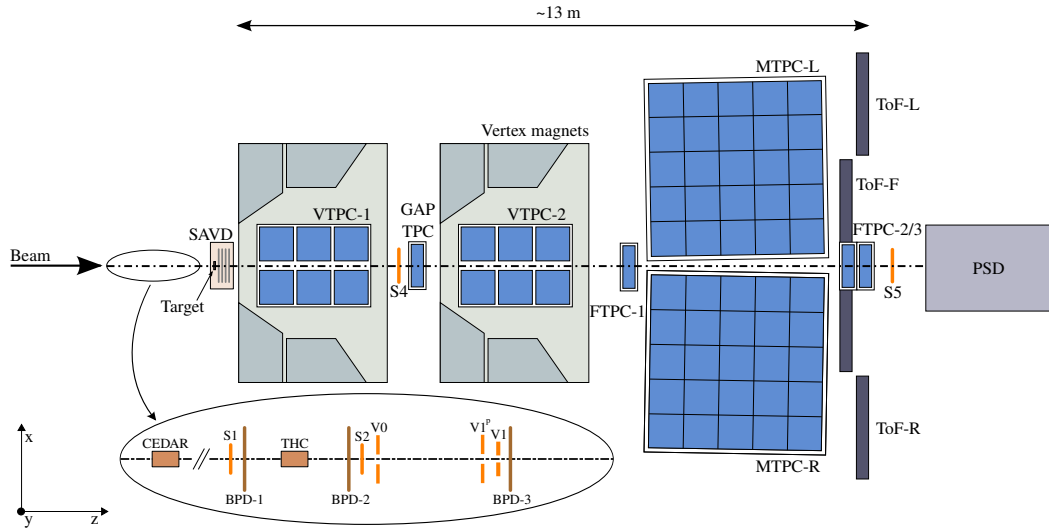


Figure 1. Schematic layout of the NA61/SHINE detection system [1].

is used to determine the centrality of the collision by the measurements of the forward energy (related to the number of projectile spectators, i.e., non-interacting projectile nucleons). The beam is monitored by beam detectors, which allows us to identify beam particles and precisely measure their trajectories.

1.3. NA61/SHINE heavy-ion program

NA61/SHINE performed a two-dimensional scan (Fig. 2) in collision energy (13A-150A GeV/c) and system size (p+p, Be+Be, Ar+Sc, Xe+La, Pb+Pb) to study the phase diagram of strongly interacting matter. The main goals of NA61/SHINE are to search for the critical point and study the onset of deconfinement. Currently, NA61/SHINE pursues the physics program focused on the open charm production measurements in order to determine the mechanism and the impact of the onset of deconfinement on it and investigate the effect of the QGP formation on J/ψ production. NA61/SHINE also pursuing physics program including measurements neutrino, and cosmic ray physics.

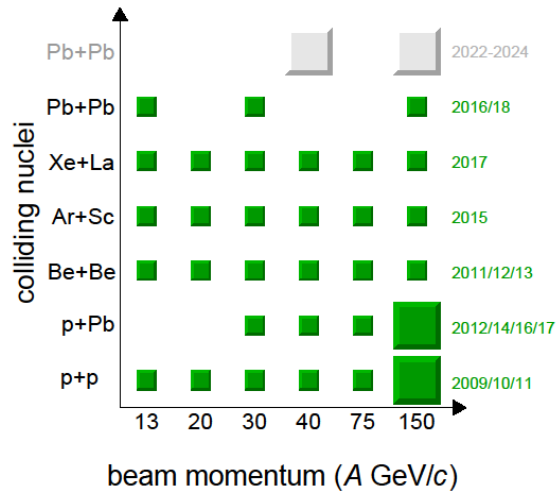


Figure 2. The NA61/SHINE beam energy and system size scan

2. Critical point search strategies

2.1. QCD critical point

A sketch of the most popular phase diagram of the strongly interacting matter is shown in Fig. 3. At low temperature (T) and baryon chemical potential (μ) the matter consists of quarks and gluons confined inside hadrons. At higher temperatures and/or baryon chemical potential, quarks and gluons may act like quasi-free particles, forming a different state of matter – Quark-Gluon Plasma (QGP). A first-order phase transition is expected between the two phases at high μ . Critical point (CP) is a hypothetical endpoint of this first-order phase transition line that has properties of second-order phase transition [2, 3].

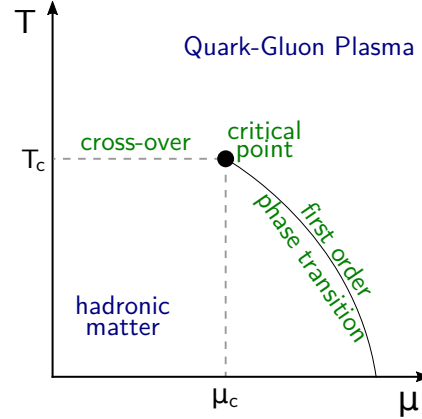


Figure 3. A sketch of the phase diagram of strongly interacting matter.

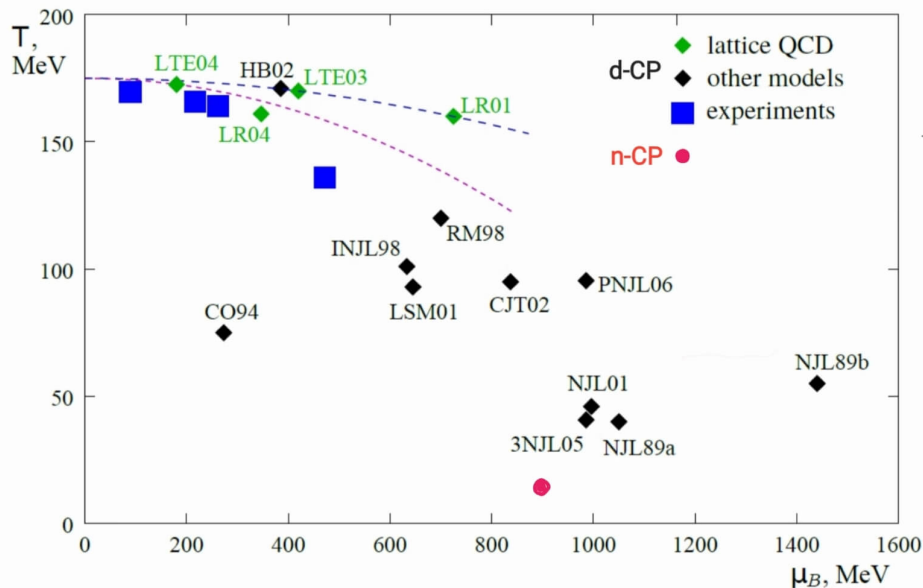


Figure 4. Compilation of theoretical predictions [4] and experimental hints [5] on the location of the deconfinement critical point, d-CP, in the phase diagram of strongly interacting matter. The position of the nuclear critical point, n-CP, as suggested by theoretical and experimental results, is indicated for comparison.

It is expected that the QCD critical point should lead to an anomaly in fluctuations

in a narrow domain of the phase diagram. However, predictions on the CP existence (Fig. 4), its location and what and how should fluctuate are model-dependent [4].

2.2. Exploring the phase diagram with heavy-ion collisions

The experimental search for the critical point requires a two-dimensional scan in freeze-out parameters (T, μ_B) by changing collision parameters controlled in the laboratory, i.e. energy and size of the colliding nuclei (or collision centrality) (Fig. 5 *left*). A characteristic feature of a second-order phase transition (expected to occur at the CP) is the divergence of the correlation length. One expects a ‘hill’ of increased fluctuations in various observables in the CP vicinity (Fig. 5 *right*), see Ref. [6] for more details.

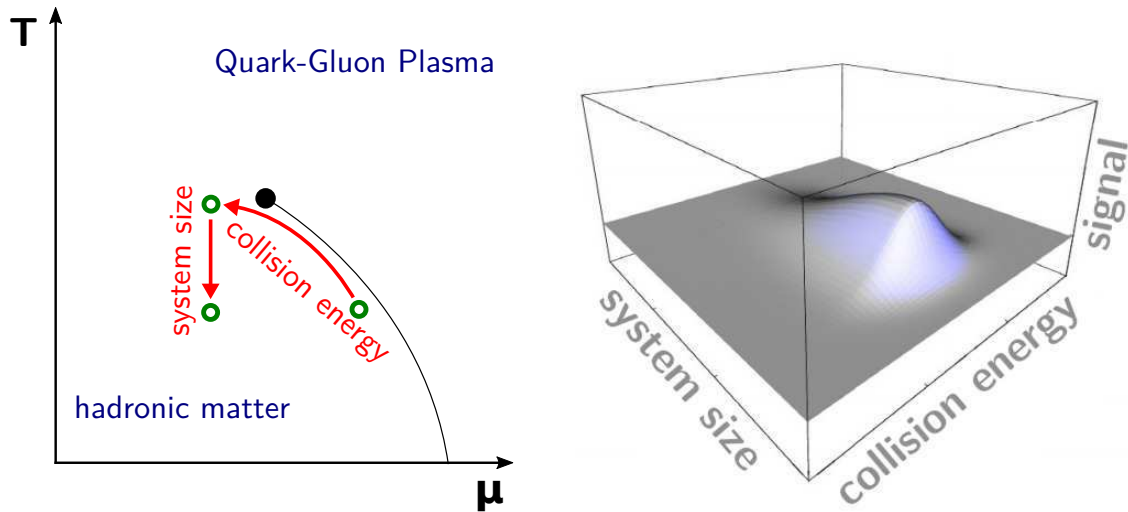


Figure 5. Hypothetical sketch of the phase diagram of strongly interacting matter with the critical point (CP), drawn as a function of baryochemical potential μ_B and temperature T (*left*), experimental search for CP requires a two-dimensional scan in freeze-out parameters (T, μ_B) by changing collision energy and system size (*left, red*). Theoretical studies predict the presence of a ‘hill of fluctuations’ as a function of colliding system size and energy for observables sensitive to the CP (*right*)

3. Experimental measures to search for critical point

The expected signal of a critical point (CP) is a non-monotonic dependence of various fluctuations (multiplicity, transverse momentum, baryon density).

3.1. Extensive quantities

An extensive quantity is a quantity that is proportional to the number of Wounded Nucleons (W) in the Wounded Nucleon Model [7] (WNM) or volume (V) in the Ideal Boltzmann Grand Canonical Ensemble (IB-GCE). The most popular is particle number

(multiplicity) distribution $P(N)$ cumulants:

$$\begin{aligned}\kappa_1 &= \langle N \rangle, \\ \kappa_2 &= \langle (\delta N)^2 \rangle = \sigma^2, \\ \kappa_3 &= \langle (\delta N)^3 \rangle = S\sigma^3, \\ \kappa_4 &= \langle (\delta N)^4 \rangle - 3\langle (\delta N)^2 \rangle^2 = \kappa\sigma^4.\end{aligned}$$

These multiplicity cumulants characterize the shape of multiplicity distribution and quantify fluctuations.

3.2. Intensive quantities

The ratio of any two extensive quantities is independent of W (WNM) or V (IB-GCE) for an event sample with fixed W (or V) – it is an intensive quantity. For example:

$$\langle A \rangle / \langle B \rangle = W \cdot \langle a \rangle / W \cdot \langle b \rangle = \langle a \rangle / \langle b \rangle,$$

where A and B are any extensive event quantities, i.e. $\langle A \rangle \sim W$, $\langle B \rangle \sim W$ and $\langle a \rangle = \langle A \rangle$ and $\langle b \rangle = \langle B \rangle$ for $W = 1$.

Popular examples are:

$$\begin{aligned}\kappa_2/\kappa_1 &= \omega[N] = \frac{\sigma^2[N]}{\langle N \rangle} = \frac{W \cdot \sigma^2[n]}{W \cdot \langle n \rangle} = \omega[n] \text{ (scaled variance),} \\ \kappa_3/\kappa_2 &= S\sigma, \\ \kappa_4/\kappa_2 &= \kappa\sigma^2.\end{aligned}$$

3.3. Strongly intensive quantities

For an event sample with varying W (or V), cumulants are not extensive quantities anymore. For example:

$$\kappa_2 = \sigma^2[N] = \sigma^2[n] \langle W \rangle + \langle n \rangle^2 \sigma^2[W].$$

However, having two extensive event quantities, one can construct quantities independent of the fluctuations of W (or V). Popular examples include [8, 9]:

$$\begin{aligned}\langle K \rangle / \langle \pi \rangle, \\ \Delta[N, P_T] &= (\omega[N] \langle P_T \rangle - \omega[P_T] \langle N \rangle) / c, \\ \Sigma[N, P_T] &= (\omega[N] \langle P_T \rangle + \omega[B] \langle N \rangle - 2(\langle NP_T \rangle - \langle P_T \rangle \langle N \rangle)) / c,\end{aligned}$$

where $P_T = \sum_{i=1}^N p_{T,i}$ and c is any extensive quantity (e.g. $\langle N \rangle$).

3.4. Fluctuations as a function of momentum bin size

When a system crosses the second-order phase transition, it becomes scale-invariant, which leads to a power-law form of the correlation function. This phenomenon leads

to enhanced multiplicity fluctuations with special properties that can be revealed by scaled factorial moments (SFMs). The SFMs are calculated by partitioning a region of transverse momentum space into a lattice of $M \times M$ bins of equal size:

$$F_r(M) = \frac{\left\langle \frac{1}{M^2} \sum_{i=1}^{M^2} n_i (n_i - 1) \dots (n_i - r + 1) \right\rangle}{\left\langle \frac{1}{M^2} \sum_{i=1}^{M^2} n_i \right\rangle^r},$$

where n_i is the number of particles in i -th bin, M^2 is the total number of bins, and averaging is done over bins and events ($\langle \dots \rangle$).

In the case of a system exhibiting critical fluctuations, $F_r(M)$ is expected to exhibit a power-law dependence on M [10, 11, 12, 13, 15]

$$F_r(M) \sim M^{D \cdot \phi_r},$$

where D is the embedding dimension (for the transverse plane, $D = 2$). Also, the exponent (intermittency index), ϕ_r is expected to obey the relation:

$$D \cdot \phi_r = (r - 1) \cdot d_r,$$

where the anomalous fractal dimension d_r is independent of r .

3.5. Scaled factorial moments in the Wounded Nucleon Model

In the Wounded Nucleon Model, $N = \sum_{i=1}^W n_i$, where W is number of wounded nucleons (constant). Also $\langle N \rangle = W \cdot \langle n \rangle$ and $\omega[N] = \omega[n]$ (scale variance). The Second Scaled Factorial moment becomes:

$$F_2[N] = \frac{1}{W} F_2[n] + 1 - \frac{1}{W}.$$

$F_2[N]$ is neither extensive ($\approx W$), nor intensive but in the limit $F_2[n] \gg 1$, $W \gg 1$:

$$F_2[N] = \frac{1}{W} F_2[n],$$

Scaled Factorial Moment is inversely extensive.

4. Experimental results

4.1. Multiplicity fluctuations

Results on the energy dependence of multiplicity fluctuations by NA61/SHINE [16] quantified by κ_4/κ_2 are presented in Fig. 6 (*left*). No prominent structures that could be related to the critical point are observed.

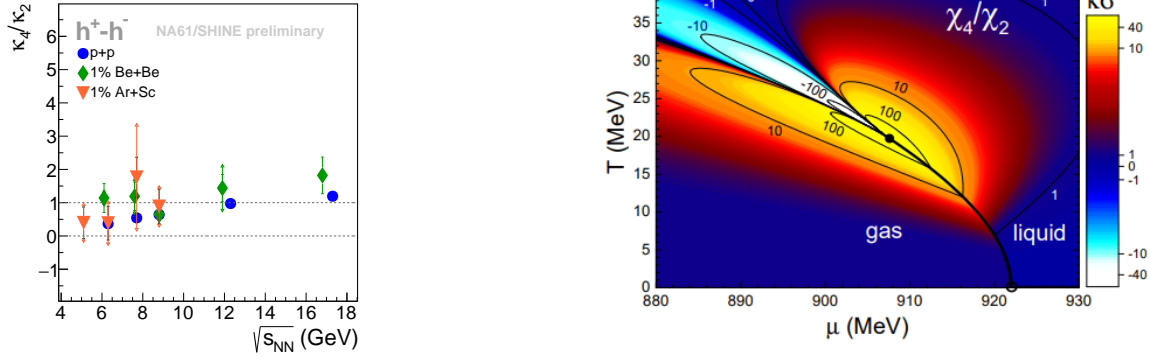


Figure 6. κ_4/κ_2 measured by NA61/SHINE [16] in inelastic $p+p$ interactions and central Be+Be, Ar+Sc collisions at the CERN SPS energies. Critical fluctuations in model with Van der Waals interaction [17] (*right*)

4.2. Multiplicity-transverse momentum fluctuations

Results on the energy dependence of multiplicity-transverse momentum fluctuations by NA61/SHINE [18] expressed in $\Sigma[P_T, N]$, strongly intensive quantity, are presented in Fig. 7. No prominent structures that could be attributed to the critical point are observed.

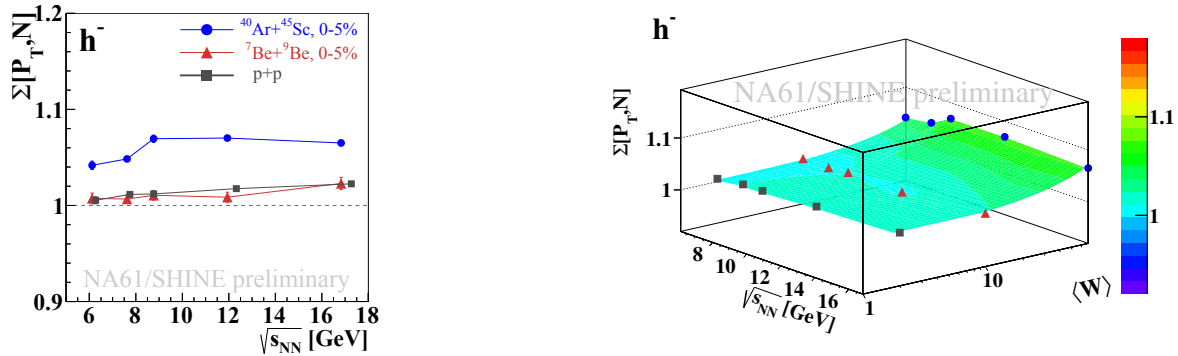


Figure 7. $\Sigma[P_T, N]$ measured by NA61/SHINE in inelastic $p+p$ interactions and violent Be+Be, Ar+Sc collisions at the CERN SPS energies. Results refer to negatively charged hadrons at forward rapidity ($0 < y_\pi < y_{beam}$) and $p_T < 1.5$ GeV/c.

4.3. Fluctuations as a function of momentum bin size (intermittency analysis)

The second Scaled Factorial Moment in transverse momentum space of mid-rapidity protons has been studied. The methodologies of using independent data points as well as cumulative quantities have been applied, as will be explained in detail below. Also, intermittency analysis of negatively charged hadrons (h^-) with Scaled Factorial Moments up to the 4th order have been studied.

4.3.1. Cumulative transformation: Scaled Factorial Moments strongly depend on the single-particle transverse momentum distribution. There are two possible ways to minimize it. First, construct mixed event data set by mixing particles from the recorded data such that each mixed event consists of particles from different data events. Then the scaled-factorial moment of mixed data should be subtracted from the recorded data. The other possibility is to transform transverse momentum components, p_x and p_y , into their cumulative equivalents [19]. This transforms non-uniform distributions into uniform from 0 to 1, preserving. (approximately) the power-law relation [20].

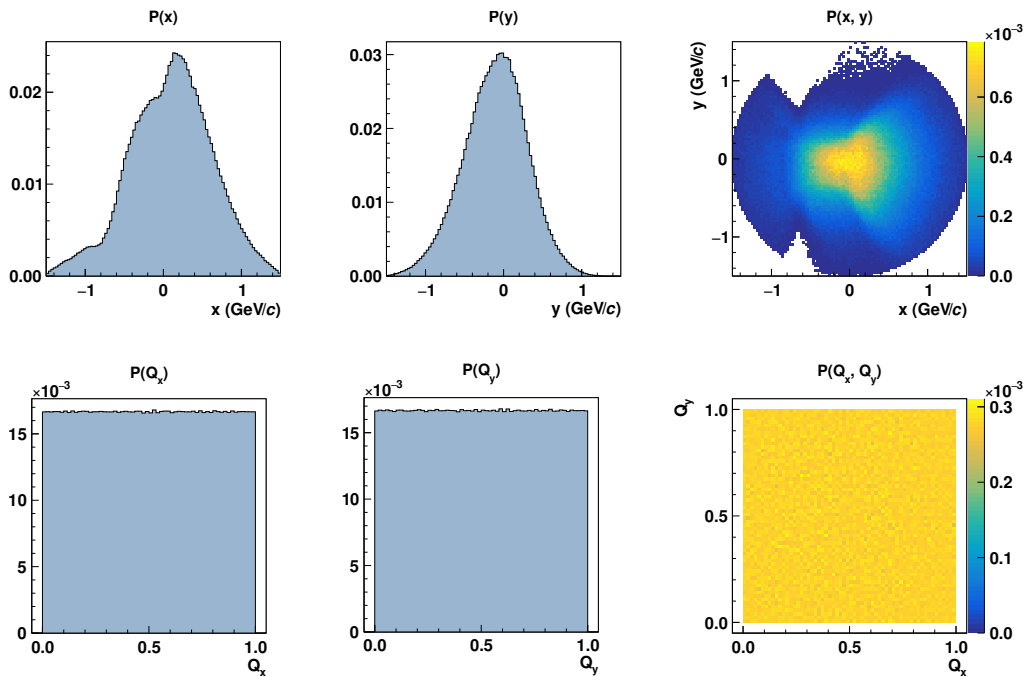


Figure 8. Example of the effect of the cumulative transformation of transverse momentum components, p_x and p_y , of proton candidates selected for intermittency analysis of NA61/SHINE Ar+Sc at 150A GeV/c data. Distributions before (*top*) and after (*bottom*) the transformation are presented.

An example of the effect of the transformation is shown in Fig. 8. Initial transverse momentum components, x and y , have been transformed into their cumulative equivalents, Q_x and Q_y . As a result, their non-uniform distributions became uniform between 0 and 1.

4.3.2. Proton intermittency results: In Fig. 9, results on the dependence of the Second Scaled Factorial Moments of proton multiplicity distributions in mid-rapidity for 0-20% most central inelastic Ar+Sc at 150A GeV/c ($\sqrt{s_{NN}} \approx 17$ GeV) and 0-10% most central Pb+Pb at 30A GeV/c ($\sqrt{s_{NN}} \approx 7.5$ GeV) collisions are presented. Each of the ten points is calculated using a fraction of the total available statistics (independent points), and cumulative transverse momentum components were used.

A separate study [21] has shown that the momentum resolution of the detector may substantially distort the power-law form of $F_2(M)$ for very small bin sizes. Therefore, $F_2(M)$ was analyzed in two ranges of momentum bin sizes, i.e. from 1 to 150 (Fig. 9, *top*) and from 1 to 32 (Fig. 9, *bottom*). No indication of a power-law increase in the number of bins is observed.

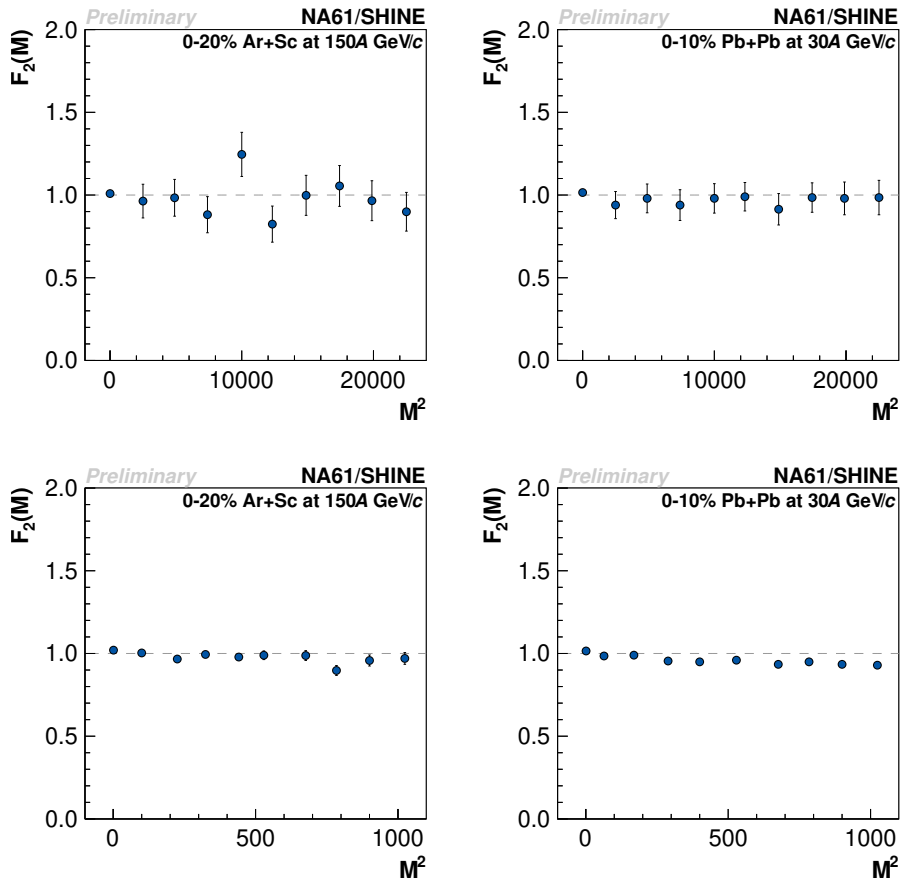


Figure 9. Results on the dependence of the second scaled factorial moment of the mid-rapidity proton multiplicity distributions for Ar+Sc at 150A GeV/c (*left*) and Pb+Pb at 30A GeV/c (*right*). Results were obtained for M from 1 to 150 (*bottom*) and 1 to 32 (*top*). Only statistical uncertainties are shown.

4.3.3. Comparison with a power-law model: Results are compared with a power-law model [22]. It generates momenta of uncorrelated and correlated protons in events with a given multiplicity distribution. The model has two controllable parameters: the fraction of correlated particles and the strength of the correlation (the power-law exponent). Using the power-law model, many high statistics data sets with multiplicity distributions identical to the experimental data and similar inclusive transverse momentum distributions have been produced. Each data set has a different fraction of correlated particles (varying from 0 to 4%) and/or a different power-law exponent (varying from 0.0 to 1.0). Next, all these generated data sets have been

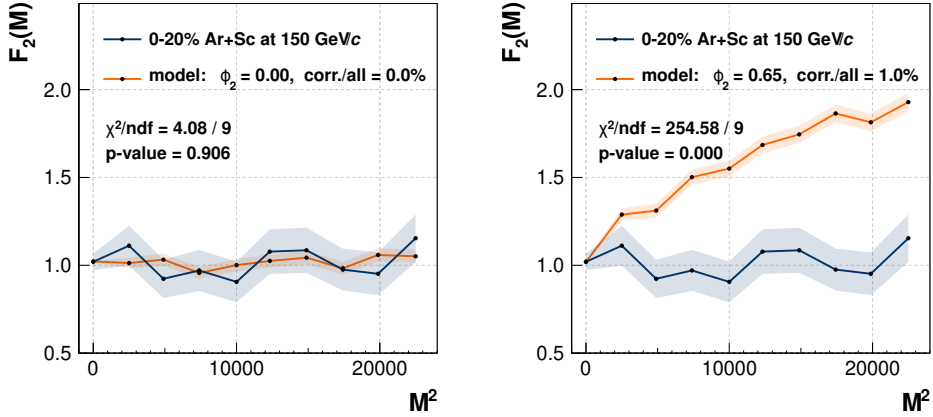


Figure 10. Example of the comparison of the simple power-law model data with experimental Ar+Sc at 150A GeV/c. No correlated particles (*left*) and 1% particles correlated with a power $\phi_2 = 0.65$ (*right*). Obtained χ^2 and p-value are used to construct the exclusion plot

analyzed in the same way as the experimental data. $F_2(M)$ results have been compared, and the p-value (probability of making a mistake by rejecting model parameters which do not reproduce the data) was calculated. An example of such comparisons is presented in Fig. 10. All p-values from each model data set, presented in one plot, form an exclusion

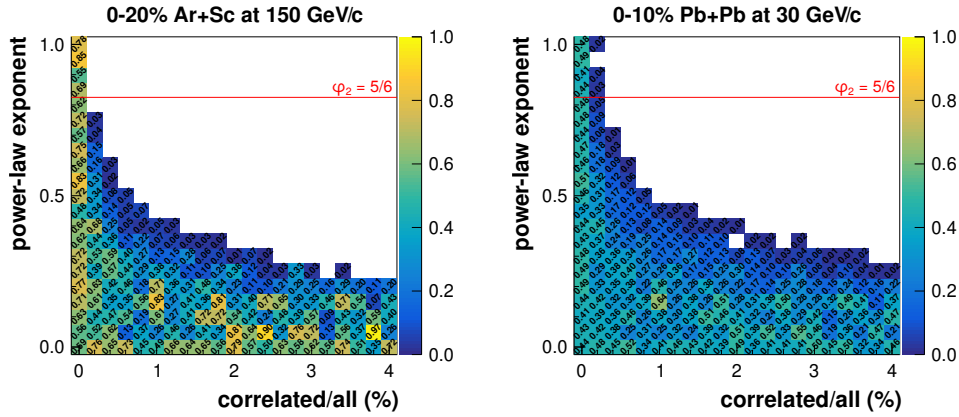


Figure 11. Exclusion plots: p-values for comparisons of $F_2(M)$ for Ar+Sc at 150A GeV/c (*left*) and Pb+Pb at 30A GeV/c (*right*) data with simple power-law model data sets with various values of two parameters (fraction of correlated particles and power-law exponent). White areas correspond to the p-value of less than 1%. Theoretical prediction for the power value for a system freezing out at the QCD critical point is marked with the red line.

plot (Fig. 11). The color scale is related to the probability that the model data set for a given number of correlated particles and a given power might be describing the data. White areas correspond to the p-value of less than 1% and may be considered excluded (for this particular model). The intermittency index ϕ_2 for a system freezing out at the

QCD critical point is expected to be $\phi_2 = 5/6$, assuming that the latter belongs to the 3-D Ising universality class.

4.3.4. Negatively charged hadron(h^-) intermittency result: In Fig. 12, h^- result on the dependence of the Scaled Factorial Moments up to 4th order of mid-rapidity h^- multiplicity distributions for 0-10% most central Pb+Pb at 30A GeV/c collisions. Each of the ten points is calculated using a fraction of the total available statistics, and cumulative transverse momentum components were used. No indication of a power-law increase in the number of bins is observed.

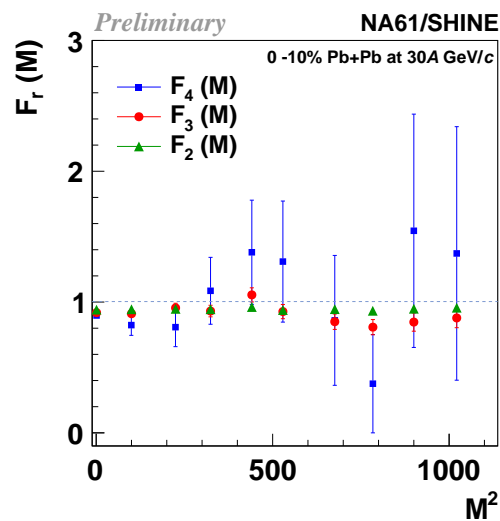


Figure 12. Results on the scaled factorial moments' dependence on the mid-rapidity h^- multiplicity distributions for Pb+Pb at 30A GeV/c. The result obtained for M from 1 to 32 up to 4th order scaled factorial moments. Only statistical uncertainties are shown.

5. Summary

NA61/SHINE experimental results on QCD critical point search have been presented. No prominent structures that could be attributed to the QCD critical point are observed in the results on multiplicity and multiplicity-transverse momentum fluctuations. No power-law increase was observed via proton and negatively charged hadron intermittency analysis of Pb+Pb at 30A GeV/c and proton intermittency analysis of Ar+Sc at 150A GeV/c data. The exclusion plot for the parameters of the power-law model (Fig. 11) for Ar+Sc at 150A GeV/c and Pb+Pb at 30A GeV/c was obtained.

6. Acknowledgments

This work is supported by the National Science Centre, Poland, under grant no. 2018/30/A/ST2/0026.

7. References

- [1] N. Abgrall, et al. J. Inst. 9 (2014) P06005.
- [2] M. Asakawa and K. Yazaki, Nucl. Phys. A **504**, 668 (1989).
- [3] A. Barducci, R. Casalbuoni, S. De Curtis, R. Gatto and G. Pettini, Phys. Lett. B **231**, 463 (1989).
- [4] M. A. Stephanov, PoS LAT **2006**, 024 (2006).
- [5] T. Czopowicz, “Overview of experimental critical point search,” in 18th International Conference on Strangeness in Quark Matter, 1 2020.
- [6] M. Gazdzicki, P. Seyboth, Acta Phys. Pol. B **47**, 1201 (2016)
- [7] A. Bialas, M. Bleszynski and W. Czyz, Nucl. Phys. B **111**, 461 (1976).
- [8] M. I. Gorenstein and M. Gazdzicki, Phys. Rev. C **84**, 014904 (2011).
- [9] M. Gazdzicki, M. I. Gorenstein and M. Mackowiak-Pawlowska, Phys. Rev. C **88**, no. 2, 024907 (2013).
- [10] J. Wosiek, Acta Phys. Polon. B**19**, 863 (1988).
- [11] A. Bialas and R. C. Hwa, Phys. Lett. B **253**, 436 (1991).
- [12] A. Bialas and R. B. Peschanski, Nucl. Phys. B **273**, 703 (1986).
- [13] N. G. Antoniou, F. K. Diakonou, A. S. Kapoyannis and K. S. Kousouris, Phys. Rev. Lett. **97**, 032002 (2006).
- [14] K. J. Sun, L. W. Chen, C. M. Ko and Z. Xu, Phys. Lett. B **774**, 103 (2017).
- [15] E. Shuryak and J. Torres-Rincon, Nucl. Phys. A **982**, 831 (2019).
- [16] M. Gazdzicki [NA61/SHINE Collaboration], PoS CPOD **2017**, 012 (2018)
- [17] V. Vovchenko, D. V. Anchishkin, and M. I. Gorenstein, J. Phys. **A48**, 305001 (2015)
- [18] E. Andronov [NA61/SHINE Collaboration], Acta Phys. Polon. Supp. **10** 449 (2017).
- [19] A. Bialas and M. Gazdzicki, Phys. Lett. **B 252** (1990), 483-486
- [20] N. Antoniou, F. Diakonou, <https://indico.cern.ch/event/818624/>
- [21] S. Samanta, T. Czopowicz, M. Gazdzicki, Nucl. Phys. **A 1015** (2021) 122299
- [22] S. Samanta, T. Czopowicz, M. Gazdzicki, J. Phys. **G 48** (2021) 10, 105106